The Finite Element Method for the Elasticity of Micro-pores Material

ARMAN ARMAN[1], ROSLIANA ESO[2,*]
[1]Department of Mathematics,
Universitas Halu Oleo,
INDONESIA

[2]Department of Physics Education,
Universitas Halu Oleo,
INDONESIA

[*]*Corresponding Author*

Abstract: -This study aimed to investigate micro-pores' impact on the elastic energy of materials using open-source simulation. The finite element method analyzed linearly elastic, homogeneous, and isotropic materials. The domain is modeled as an isotropic elastic material with a constant thickness and is treated as a two-dimensional rectangular plate. The positions and diameters of the micro-pores were varied. The results indicate that the position and diameter of the micro-pores within the domain significantly influence the magnitude of elastic energy. Larger pore diameters correspond to higher values of elastic energy. Additionally, the elastic energy value of the micro-pores remains relatively constant, though it is smaller when the pores are located at the ends of the material. This suggests that the elasticity at the end of the material is reduced due to pressure-induced movement. Furthermore, varying the diameter of the micro-pores leads to more noticeable changes in material shape, with larger diameters resulting in more pronounced alterations.

Key-Words: - Finite element method, Elastic energy, Isotropis, Rectangular plate, Open-source simulation, and Micro-porous material.

Received: September 9, 2023. Revised: May 15, 2024. Accepted: June 11, 2024. Published: July 26, 2024.

1 Introduction

Mechanical properties such as elastic modulus of materials can be affected by variations in pore shape and distribution, [1]. Micromechanical modeling mostly focuses on practical changes in the shape of a material, which is usually determined by various factors such as ultimate strength, Young's modulus, and Poisson's ratio, [2]. Micromechanical modeling for predicting the linearly elastic limit properties also extends to effective stress-strain behavior beyond the tensile flow stress in anisotropic sheet samples, [3]. Apart from the material's length, width, and thickness, the micro-pore effect is also part of the geometric effect, which contributes significantly to the change in the shape of the material. It should be noted that the microstructure of porous materials in practical existence consists of pores distributed irregularly in various sizes and shapes. In particular, the distribution mode of these pores also clearly affects the overall elasticity of the material, [4]. The difference in the arrangement and distribution of the pore structure plays a vital role in optimizing the pore topology and achieving the desired effective material properties or tailoring specific textures, [5].

Recent experimental findings show that stress transfer increases with increasing porosity [6], suggesting that numerical modeling only considers idealized pore arrangements. Hence, the stress induced by the external excitations can be transferred more smoothly in this microstructure but provides physical insight into how microscopic porous shapes affect macroscopic mechanical responses through systematic analysis. This feature may give novel ideas for designing porous structures or bio-implants with specific requirements, [7]. The use of approaches on a uniaxial compression of micro-porous rubber [8], compared with the experimental data for the stress–stretch and volume change–stretch data of elastomers in uniaxial tension [9] under certain conditions for physical background and characteristic behavior found that the constitutive response of an elastic material offers different insights about the observed elasticity micro-pores phenomenon.

In this study, we focus on the shape of the material and the elastic properties of the micro-porous material, which are only isotropic, with uniaxial stress tensors considered, [10]. The initial and boundary conditions could be the same for subsystems, which requires the assumption that both subsystems receive the exact amounts of pressure. Numerical techniques can be conveniently utilized to analyze porous structural materials with vacancies, [11]. We also assume that the stress tensors are equal and that the model requires information about the material structure, especially its components. We can find local solutions following these patches to divide the computational region into illustrations and individual small patches, obtaining a deformation solution using the Finite Element Method (FEM), [12], [13], [14], [15]. However, one needs proficiency in matrix algebra and good computer commands to apply powerful tools to engineering problems and obtain valuable solutions.

2 Numerical Formulation

In this paper, we denote the gradient and divergence concerning $x = (x_1,x_2)^T \in \mathbb{R}^2$ by ∇ and div, respectively. We denote the Lebesgue space on Ω by $L^2(\Omega)$ and the $\mathbb{R}^2$-valued Lebesgue space by $L^2(\Omega; \mathbb{R}^2)$. We also often use the Sobolev space defined by $H^1(\Omega) := \{u \in L^2(\Omega); \nabla u \in L^2(\Omega; \mathbb{R}^2)\}$, and its trace space on the boundary Γ_D, u denotes the unknown displacement field $u(x)=((u_1(x),u_2(x))^T \in \mathbb{R}^2$. Then, the strain tensor e[u](x) is defined by $e[u](x) = e_{ij}[u](x)$

$e_{ij}[u] = e_{ji}[u] := \frac{1}{2}\left(\frac{\partial u_i}{\partial x_j} + \frac{\partial u_j}{\partial x_i}\right)$, and the stress tensor is denoted by $\sigma[u](x) = (\sigma_{ij}[u](x)) \in R_{sym}^{2x2}$ and defined as $\sigma[u] := Ce[u]$, the elasticity tensor $C(x)=(c_{ijkl}(x))$ asumed in symmetry condition, so the overall constitutive equation follows Hooke's law

$$\sigma_{ij}[u](x) := c_{ijkl}(x)e_{kl}[u](x) \quad (1)$$

If the representative volume element is assumed homogeneous, isotropic and linearly elastic, then $c_{ijkl}(x)$ or anisotropic elastic tensor expressed as $c_{ijkl}(x) = \lambda\delta_{ij}\delta_{kl} + \mu\left(\delta_{ik}\delta_{jl} + \delta_{il}\delta_{jk}\right)$. Here, λ and μ are Lame constant and δ_{ij} is a delta cronecker, so eq (1) become:

$$\sigma_{ij} = \lambda e_{kk}\delta_{ij} + 2\mu e_{ij} \quad (2)$$

For each elastic fracture mechanics, a small displacement represents deformation[16] where the superscript T denotes the transposition, equation 2 be written as:

$$\sigma[u] = \lambda(div\, u)I + 2\mu e[u]$$
$$tr\ \sigma[u] = (3\lambda + 2\mu)\ div\ u,$$
$$\sigma_{ij}[u] = (3\lambda + 2\mu)e_{ii}[u] \quad (3)$$

Therefore, the strain component can be expressed as a function of the stress component in eq.3 by combining:

$$e_{ij}[u] = \frac{1}{2\mu}\sigma_{ij}[u] - \frac{\lambda}{2\mu(3\lambda + 2\mu}\ tr\ \sigma_{kk}[u]\delta_{ij}$$

If the stress tensor is uniaxial, $\sigma_{11} = \sigma$, and $\sigma_{22} = \sigma_{33} = \sigma_{12} = \sigma_{23} = \sigma_{31} = 0$, the corresponding strain comp $e_{12} = e_{23} = e_{31} = 0$, then $e_{11} = \frac{1}{\mu}\frac{\lambda+2\mu}{(3\lambda+2\mu}\ [u]$,

$$e_{22} = e_{33} = \frac{-\lambda}{2\mu(3\lambda + 2\mu}\ [u]$$

Young's modulus and Poisson's ratio defined as:

$$E = \frac{\sigma_{11}}{e_{11}} = \frac{\mu(3\lambda + 2\mu)}{\lambda + \mu}, v = \frac{e_{22}}{e_{11}} = \frac{\lambda}{2(\lambda + \mu)}$$

the Lame constant form:

$$\lambda = \frac{E\upsilon}{(1+\upsilon)(1-2\upsilon)}, \mu = \frac{\lambda}{2(1+\upsilon)} \quad (4)$$

Assume that an elastic body occupies the domain volume Ω and let ω be a subdomain of Ω with boundary Γ_D and normal vector n, concerning the elastic equilibrium equation defined as [17],

$$\Sigma F = \int_{\widetilde{\Omega}} f dx + \int_{\omega} \sigma \cdot n ds = 0 \quad (5)$$

Then, in purely elastic materials assuming, by using the divergence theorem the linear elasticity equation in eq (5) can generally be expressed in terms of partial differential equations governing deformation and stress a slight displacement gradient

$$-div(\sigma[u]) = f(x) \quad x \in \Omega \quad (6)$$
$$u = g\,(x),\ x \in \Gamma_D, u \in x|u_{\Gamma_D} = g_{\Gamma_D},$$
$$\sigma[u] \cdot n = q(x) \quad x \in \Gamma_N\ ,$$

Then, $f \in L^2(\Omega; R^2);\ q \in L^2(\Gamma_N; R^2); \sigma \in R_{sym}^{2x2}$,
$x := H^1(\Omega;\ R^2) = \{u = \Omega \to R^3 | u_i \in H^1(\Omega)\}$

where f(x) is a given external load perpendicular to the plate on Ω, g(x) is a given anti-plane displacement on Γ_D, and q(x) is a given boundary load in the x3-direction on Γ_N . The outward normal derivative on the boundary of Ω is denoted by $\partial/\partial n$. Transformation of the model to the non-dimensional system was using the Finite Element

Methods (FEM) with assumptions, $\tilde{x} = \frac{x}{L_R}$, $\tilde{x} \in \tilde{\Omega}$, then,

Assuming that this functional system is also appropriate for the pore diameter and can express the existence of parallel channels with variations in the location/position of the material pores, the problem may now be written in the weak formulation, [18]. For this purpose, we multiply the differential in equation (6) with the so-called test function v, which, $v \coloneqq \{u \in x \,|u_{\Gamma_D} = (0,0,0)^T\} \subset x$ and if $g \in x$, $u|_{\Gamma_D} = 0$, and integrate both sides over the whole domain Ω , therefore,

$$\int_{\tilde{\Omega}} f \bullet v \, dx = -\int_{\tilde{\Omega}} \tilde{\nabla}\tilde{\sigma}\,[\tilde{u}] \bullet v \;\; dx. \qquad (7)$$

If we require the test function v to satisfy the same boundary condition, $v|_{\Gamma_D} = 0$, by using the Divergence Theorem, equation (6) becomes

$$\int_{\tilde{\Omega}} f \bullet v \, dx \, f \bullet v \, dx = -\int_{\widetilde{\partial\Omega}} \widetilde{\sigma_{iJ}}\,[\tilde{u}] n_j \, v_i dS + \int_{\tilde{\Omega}} \widetilde{\sigma_{iJ}}\,[\tilde{u}]\,(\partial_j v_i)\, dx \qquad (8)$$

The displacement of v appears inside an integral. Since the integration provides a smoothing effect, $\sigma_{ij}[u]n_j v_i = (\sigma[u]n)\cdot v = q \cdot v$, need to be continuous, so the calculus comes into play for a differentiable function of the weak derivative that is equal to the usual result.

$$\int_{\Omega} \tilde{\sigma}\,[\tilde{u}]\,(\partial_j v_i)\, dx = \int_{\tilde{\Omega}} \left((div\,\tilde{u})(div(v) + 2\mu e[u]\, e[v])\right) dx \qquad (9)$$

where $\int_{\Omega} f \bullet v \, dx - \int_{\widetilde{\partial\Omega}} \tilde{q} \;.v\, dS$ is an unknown function, and $\int_{\tilde{\Omega}} \widetilde{\sigma_{iJ}}\,[\tilde{u}]\,(\partial_j v_i)\, dx = \int_{\tilde{\Omega}} \left((div\,\tilde{u})(div(v) + 2\mu e[u]\, e[v])\right) dx$ is a given function.

At time t ∈ [0, T], we denote the weak solution to (8) by u(t). Then, the weak solution u(t) is characterized by the following variational principle, i.e., it is obtained as a unique minimizer of the following elastic energy including the body and surface forces under a suitable boundary condition

$$E_{el}(t,v) \coloneqq \frac{1}{2}\int_{\tilde{\Omega}} \widetilde{\sigma_{ij}}\,[\tilde{u}]\,(\partial_j v_i)\, dx - \int_{\tilde{\Omega}} f(t).v \;\; dx - \int_{\widetilde{\Gamma_N}} \tilde{q}\,.v\, dS \qquad (10)$$

The numerical solution simulation uses FreeFem++ software, an open-source software combined with GNUplot, to perform a chart. One must define initial and boundary conditions with the plate is supposed to be an isotropic elastic material with a constant thickness and is treated as a two dimensional rectangular on the x-axis and y-axis in Ω field with the border in cartesian domain

border A(t=a1,a2) {x = t; y = b1;
border B(t=b1,b2) {x = a2; y = t;
border C(t=a2,a1) {x = t; y = b2;
border D(t=b2,b1) {x = a1; y = t;

The micropores domain restrict the *border L (t=0, 2*pi)* and the domain position can vary to very diverse diameter systems showed in Figure 1.

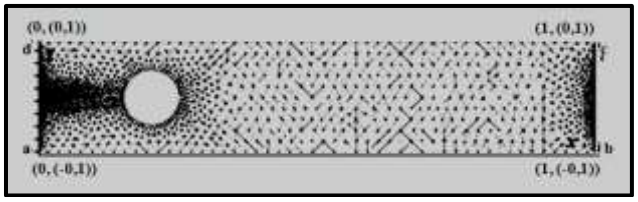

Fig. 1: Numerical domain on the cartesian plane

The first design is to determine different pore positions (h), namely h1= (0.2) μm h2= (0.4,) μm, h3= (0.6) μm and h4= (0.8) μm. After that, the pore diameter (d) was varied at each different pore position from the value range 0.01 μm ≤d≤ 0.09 μm. The second design used four materials with different pore diameters (d): 0.02 μm, 0.04 μm, 0.06 μm, and d4 = 0.08 μm. The pore position (h) was varied for each pore diameter. The parameters Young's modulus (λ) and Poisson's ratio (μ) [19], are written with the following code: real mu = 7.617e10; real lambda = 9.69e10; real rho = 7700; real E = 1.84e6; and real nu = 0. . Whereas the elastic linear equations are written as solvelame([u1,u2],[v1,v2]) =

```
  int2d(Th)(lambda*div(u1,u2)*div(v1,v2)
+ 2.*mu*(eps(u1,u2)'*eps(v1,v2)))
- int2d(Th)(gravity*v2)
- int1d(Th,3)(23.75*alpha*
-sin(0.3*pi*t)*v2)+on(4, u1=0, u2=0)+on(2, u2=0).
```

3 Results and Discussion

3.1 Numerical Simulation of Displacement on a Variety of Micropore Positions

Because the pores in porous materials are frequently irregularly distributed and formed in the solid phase, it is challenging to ascertain the total elastic characteristics using analytical or experimental means. For this reason, the numerical analysis becomes essential. A representative volume element

(R) is established if the porous material is considered homogenous at the macroscopic scale. The local response of the absorbent material, as determined by micromechanics, may be used in conjunction with the particular boundary condition to derive the overall moduli of porous materials. Below are the results of a displacement simulation in location (H = 0,1 ⌈m and 0,2 ⌈m) where the micro-pore diameter is varied. The results are shown in Figure 2, Figure 3, Figure 4 and Figure 5.

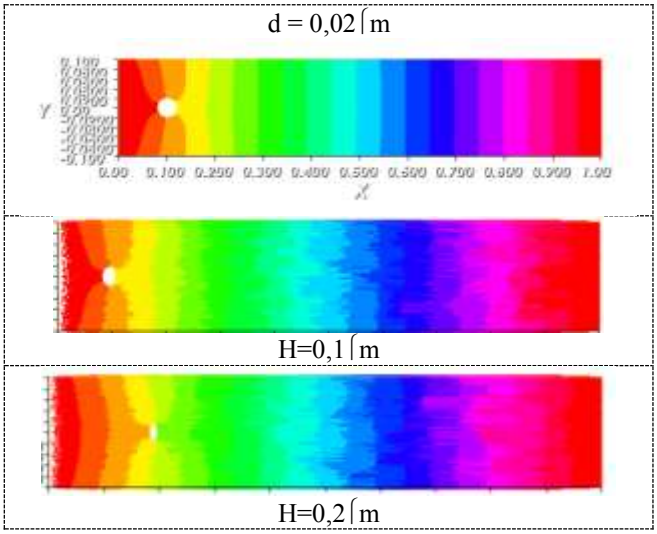

Fig. 2: Displacement simulation at micro-pore diameter of 0.2 μm

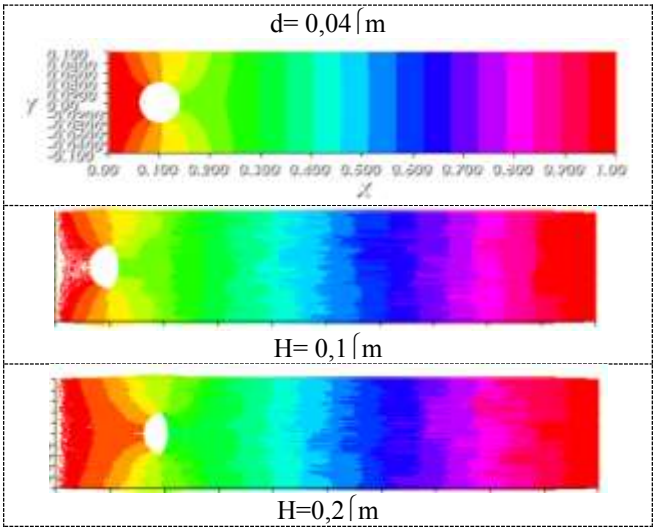

Fig. 3: Displacement simulation at micro-pore diameter of 0.4 μm

In the mixed position configuration, small circular pores oriented along the load direction play an important role compared with large ones. Discrete plastic deformation bands are sharper and essentially bypass these pores. The earlier the damage starts and, therefore, the lower elasticity can be expected.

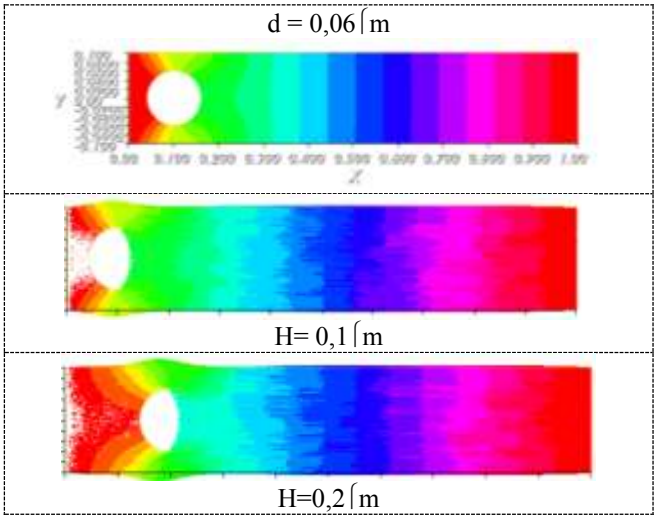

Fig. 4: Displacement simulation at micro-pore diameter of 0.6 μm

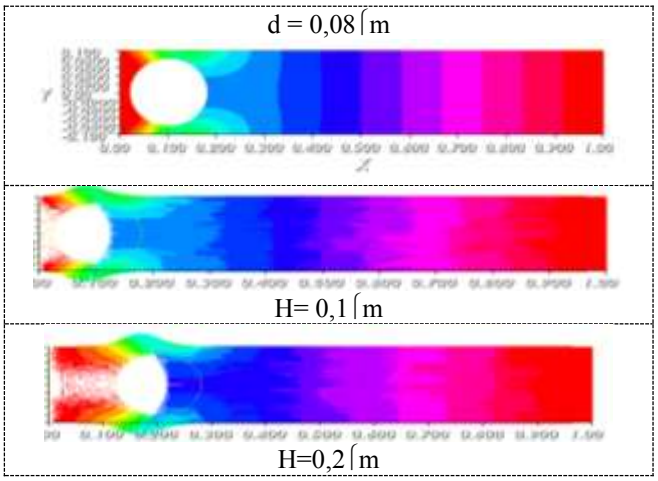

Fig. 5: Displacement simulation at micro-pore diameter of 0.8 μm

3.2 Numerical Simulation of Displacement due to Change in Micropore Diameter

Displacement simulations with various micropore diameters determined by the design location micropores of H1=(0.2)μm, H2=(0.4) μm, H3=(0.6)μm, and H4=(0.8) μm are provided. The diameter (d) of the micropores was then adjusted for each separate pore size in the range of 0.01 μm to 0.09 μm. The results are shown in Figure 6, Figure 7, Figure 8 and Figure 9.

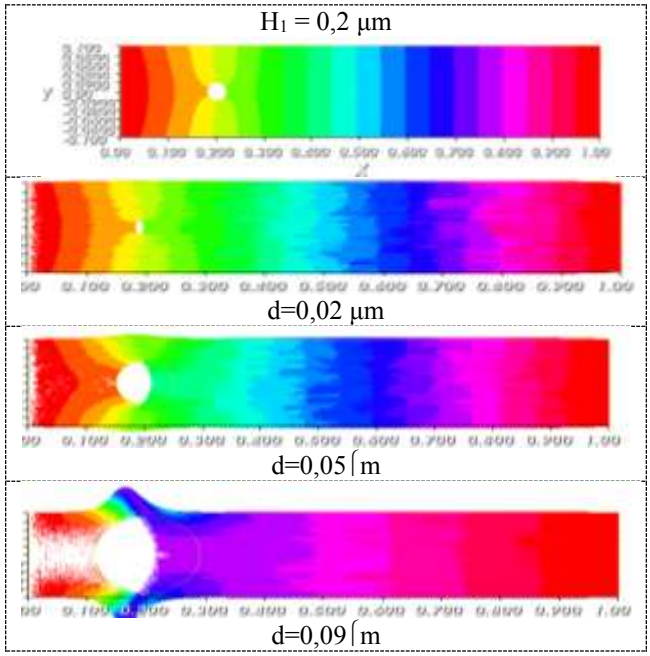

Fig. 6: Simulated displacement of micropores at H1=0.1 µm, diameter varied from 0.01 to 0.09 µm

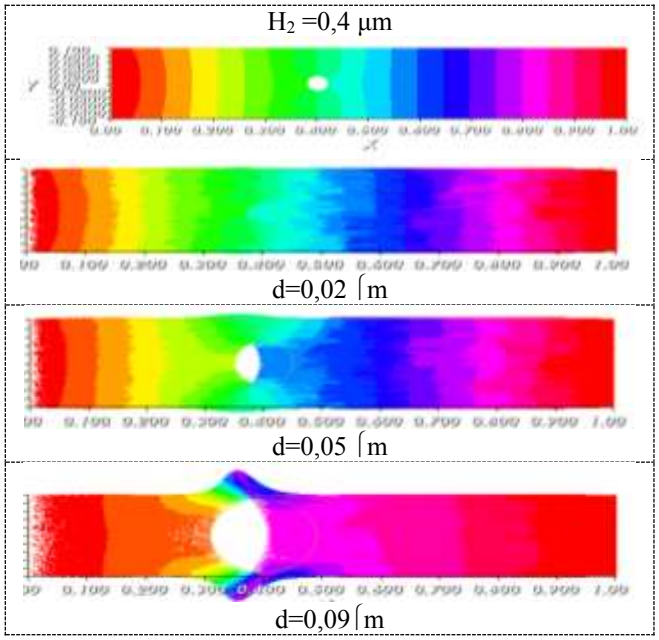

Fig. 7: Simulated displacement of micropores at H2=0.4 µm, diameter varied from 0.01 to 0.09 µm

A rectangular material with micropores is seen in the above photograph. The top and lower ends of the micropores in the material broaden as the micropores' diameter varies; the higher the micropores' diameter, the larger the shape of the material changes. Based on the strain energy function of microporous materials under uniaxial compression, a volumetric strain energy function is produced, taking into account the mathematical link between strain energy and the impact of porosity on the relationship between stress and strain. The simulation results for this area may be used to calculate the energy level sufficient to achieve the elastic value, and a graphical representation of the results is required. The graph in Figure 10 shows the elastic energy level as a consequence of the microporous region's pore location and pore size.

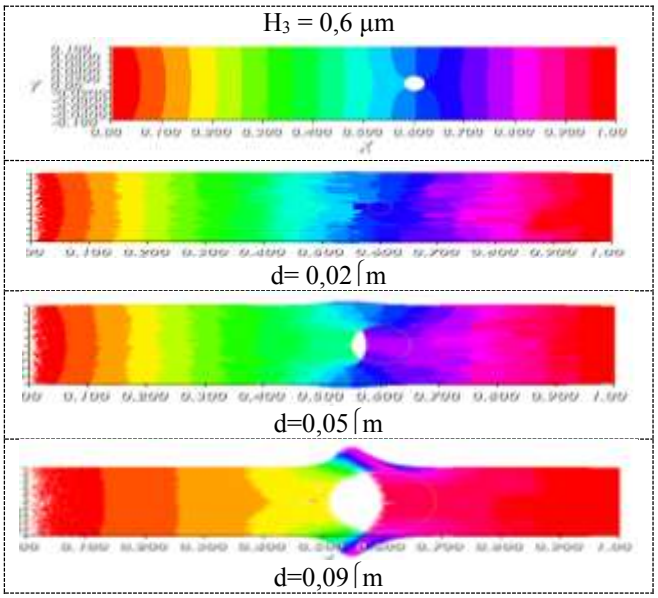

Fig. 8: Simulated displacement of micropores at H3=0.6 µm, diameter varied from 0.01 to 0.09 µm

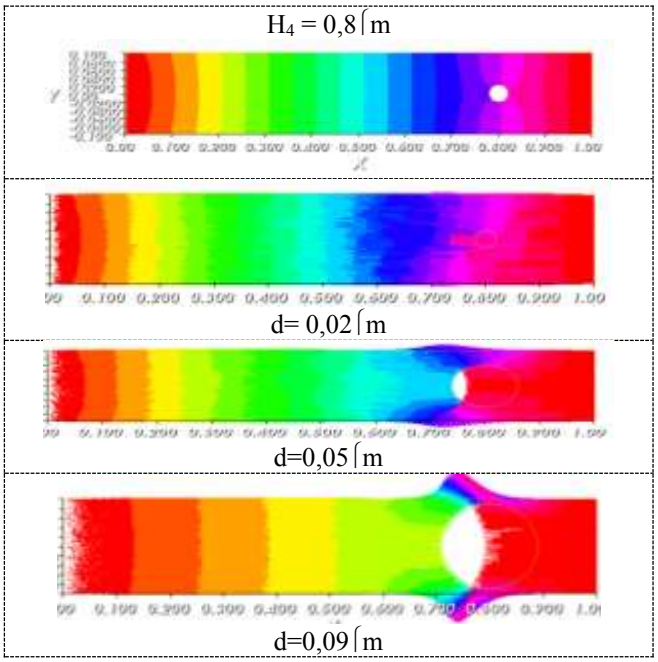

Fig. 9: Simulated displacement of micropores at H4=0.8 µm, diameter varied from 0.01 to 0.09 µm

A rectangular material with micropores is seen in the above photograph. The top and lower ends of the micropores in the material broaden as the micropores' diameter varies; the higher the micropores' diameter, the larger the shape of the

material changes. Based on the strain energy function of microporous materials under uniaxial compression, a volumetric strain energy function is produced, taking into account the mathematical link between strain energy and the impact of porosity on the relationship between stress and strain. The simulation results for this area may be used to calculate the energy level sufficient to achieve the elastic value, and a graphical representation of the results is required. The graph in Figure 10 shows the elastic energy level as a consequence of the microporous region's pore location and pore size.

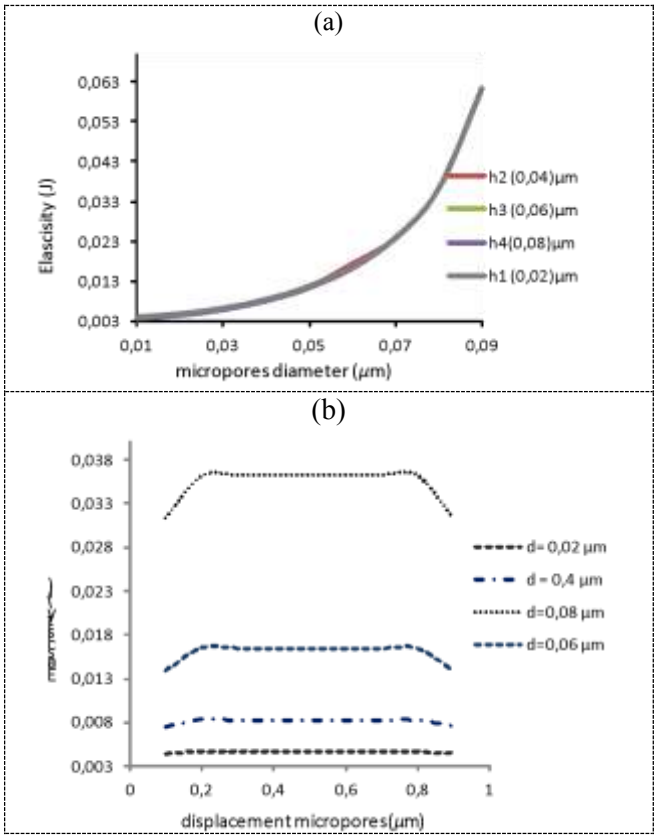

Fig. 10: Elastic energy of micropores: (a) varied in pore displacement and (b) varied in pore diameter

Elasticity has been shown to increase with the diameter of the micropores, indicating that differences in the size of the micropores affect the elastic value of the material. The elastic value is almost constant when the micropores shift to different positions, but the value decreases when the micropores are at both ends of the material, indicating that the elasticity at the ends of the rectangular material is smaller than when the micropores are located in the middle of the content. The greater the pore diameter, the greater the elasticity energy value. However, with variations in position, the elasticity value of the micropores is nearly constant, even though the value is small when the micropores are at the ends of the material, indicating that the elasticity at the ends of the rectangular material is smaller than when the micropores are in the middle. However, creating elasticity material would be challenging as it depends on several factors, such as the microporous position and the microporous diameter for a constituent in future investigations concerning the presented physical and mathematical aspects.

4 Conclusion

Rectangular domains with micropores have been successfully simulated using open-source software. The presence of micropores affects the ability of the material to change its shape. The greater the pore diameter, the greater the elasticity energy value. Moreover, the elasticity value of the micropores is nearly constant, even though the value is small when the micropores are at the ends of the material, indicating that the elasticity at the ends of the rectangular material is smaller than when the micropores are in the middle. It will close due to the movement of the material induced by the pressure. The larger the diameter of the microporous, the more the shape of the material changes, that is, the wider the top and bottom surfaces of the material. It would be interesting to extend the analysis of the diameter of the microporous and its distribution in homogenous domain material and the usefulness of a practical system of the material's shape change processing.

References:

[1] Y. L. Shen and N. Fathi, "Numerical study of elastic-plastic behaviour of pore-containing materials: effects of pore arrangement," *Int. J. Theor. Appl. Multiscale Mech.*, vol. 3, no. 4, p. 262, 2021. DOI: 10.1504/ijtamm.2021.120795.

[2] Ochiai, Shojiro, Satoshi Nakano, Yuya Fukazawa, Mohamed Shehata Aly, Hiroshi Okuda, Komei Kato, Takeshi Isobe, Koichi Kita, and Keiichi Honma. 2010. "Change of Young's Modulus with Increasing Applied Tensile Strain in Open Cell Nickel and Copper Foams." *Materials Transactions*, vol. 51 (5), pp 925–932. https://doi.org/10.2320/matertrans.M2009384.

[3] F. Barlat, H. Aretz, J. W. Yoon, M. E. Karabin, J. C. Brem, and R. E. Dick, "Linear transfomation-based anisotropic yield functions," *Int. J. Plast.*, vol. 21, no. 5, pp. 1009–1039, 2005. DOI:

10.1016/j.ijplas.2004.06.004.

[4] A. Srivastava, S. Osovski, and A. Needleman, "Engineering the crack path by controlling the microstructure," *J. Mech. Phys. Solids*, vol. 100, August, pp. 1-20, 2017. DOI: 10.1016/j.jmps.2016.12.006.

[5] O. Cazacu and J. A. Rodríguez-martínez, "Effects of plastic anisotropy on localization in orthotropic materials: New explicit expressions for the orientation of localization bands in flat specimens subjected to uniaxial tension," *J. Mech. Phys. Solids*, vol. 126, pp. 272–284, 2019. https://doi.org/10.1016/j.jmps.2019.03.002.

[6] T. Hung, D. Duc, T. Tu, L. Dung, and C. Bao, "Static and dynamic behaviour of sandwich beams with porous core: Experiment and moving least squares mesh-free analysis," *Journal of Science and Technology in Civil Engineering (JSTCE) - HUCE.*, vol. 18(1), pp. 39–54 2024. http://dx.doi.org/10.31814/stce.huce2024-18(1)-04.

[7] H. Li, S. Dong, J. Liu, Y. Yu, and M. Wu, "Finite Element Modeling of Porous Microstructures With Random Holes of Different-Shapes and -Sizes to Predict Their Effective Elastic Behavior," *appl. sci.*, vol. 9, pp. 1–20, 2019. Doi: 10.3390/app9214536.

[8] N. Li, H. Xu, L. Hu, X. Wang, and L. Lu, "Elastic constitutive model and compression experiment based on microporous silica composites," *Mech. Adv. Mater. Struct.*, vol. July, pp. 1–5, 2020. https://doi.org/10.1080/15376494.2020.1780353.

[9] Moerman, Kevin M. Fereidoonnezhad, Behrooz McGarry, J. Patrick, "Novel hyperelastic models for large volumetric deformations," *International Journal of Solids and Structures*, vol. 193-194, pp. 474–491,2020. https://doi.org/10.1016/j.ijsolstr.2020.01.019.

[10] Y. Yu and W. Huang, "Selection of regularization parameter in the Ambrosio-Tortorelli approximation of the Mumford-Shah functional for image segmentation," *Numer. Math.*, vol. 11, no. 2, pp. 211–234, 2018. DOI: 10.4208/nmtma.OA-2017-0074.

[11] M. Repka, V. Sládek, and J. Sládek, "Numerical Analysis of Poro-elastic Materials Described by the Micro-dilatation Theory," *Procedia Eng.*, vol. 190, pp. 248–254, 2017. DOI: 10.1016/j.proeng.2017.05.334.

[12] M. S. H. Mojumder, M. N. Haque, and M. J. Alam, "Efficient Finite Difference Methods for the Numerical Analysis of One-Dimensional Heat Equation," *J. Appl. Math. Phys.*, vol. 11, no. 10, pp. 3099–3123, 2023. DOI : 10.4236/jamp.2023.1110204.

[13] Erhunmwun, Iredia, and Usiosefe Ikponmwosa,"Review on Finite Element Method." *J. Appl.Sci.Environ.Manage* , vol. 21, no. 5, pp. 999-1002, 2018. https://doi.org/10.4314/jasem.v21i5.30.

[14] Z. Qing, Z. Jiashou, and X. Xiaozhou, "The Partitioned Mixed Model of Finite Element Method and Interface Stress Element Method with Arbitrary Shape of Discrete Block Element," *Mathematical Problems in Engineering*, vol. September, pp. 1-6, 2013. http://dx.doi.org/10.1155/2013/950696.

[15] L. Wang, S. Li, G. Zhang, Z. Ma, and L. Zhang, "A GPU-Based Parallel Procedure for Nonlinear Analysis of Complex Structures Using a Coupled FEM / DEM Approach," *Mathematical Problems in Engineering*, vol. 13, pp. 1-15, 2013. http://dx.doi.org/10.1155/2013/618980.

[16] M. Kimura, H. Notsu, Y. Tanaka, and H. Yamamoto, "The Gradient Flow Structure of an Extended Maxwell Viscoelastic Model and a Structure-Preserving Finite Element Scheme," *J. Sci. Comput.*, vol. 78, no. 2, pp. 1111–1131, 2019. https://doi.org/10.1007/s10915-018-0799-2.

[17] M. Kimura, T. Takaishi, S. Alfat, T. Nakano, and Y. Tanaka, "Irreversible phase field models for crack growth in industrial applications : thermal stress , viscoelasticity , hydrogen embrittlement," *SN Appl. Sci.*, vol. June, 2021. DOI: 10.1007/s42452-021-04593-6.

[18] J.Sladek, V. Sladek, M.Reka, P.L. Bishay, "Static and dynamic behavior of porous elastic materials based on micro-dilatation theory: A numerical study using the MLPG method," *International Journal of Solids and Structures*, vol. 96, pp. 126–135, 2016. https://doi.org/10.1016/j.ijsolstr.2016.06.016.

[19] Bischoff, J.E., Arruda, E.M., Grosh, K., "A new constitutive model for the compressibility of elastomers at finite deformations," *Rubber Chem. Technol*, vol. 74 (4), pp.541–559. 2001. DOI: 10.5254/1.3544956.

Contribution of Individual Authors to the Creation of a Scientific Article (Ghostwriting Policy)

The authors equally contributed in the research, at all stages from the formulation of the problem to the final findings and solution

Sources of Funding for Research Presented in a Scientific Article or Scientific Article Itself

No funding was received for conducting this study.

Conflict of Interest

The authors have no conflicts of interest to declare.